Journal of Hydroscience and Hydraulic Engineering
Vol. 27, No.1 May, 2009, 11-21

3D NUMERICAL PREDICTION FOR TRANSPORTATION AND ENTRAPMENT OF DRIFTWOOD WITH T-TYPE SOLID MODEL

By

Satoru Ushijima

Department of Civil and Earth Resources Engineering, Kyoto University, Kyoto-shi, 615-8540, Japan

Osashi Makino

Department of Civil and Earth Resources Engineering, Kyoto University, Kyoto-shi, 615-8540, Japan

and

Norimasa Yoshikawa

Department of Civil and Earth Resources Engineering, Kyoto University, Kyoto-shi, 615-8540, Japan

SYNOPSIS

A computational method was developed to predict the movements of driftwoods transported by three-dimensional free-surface flows. A T-type solid model, which represents a floating driftwood, is introduced into the prediction method, MICS, which enables us to deal with the free-surface flows including floating objects as a multiphase flow fields. In the T-type model, driftwood is represented by multiple tetrahedron elements and its volume, mass and inertia tensors are accurately represented with the elements. The contact forces due to the collisions of driftwoods are evaluated with the contact-spheres distributed near the surfaces of the T-type model. The MICS with the T-type model was applied to experimental results and it was shown that the movements and entrapment of driftwoods observed in the experiments are reasonably predicted with the present method.

INTRODUCTION

It is important to predict the movements of driftwoods transported by flood flows in terms of the evaluation of the flooded area and the safety of hydraulics structures. The entrapment of the driftwoods around bridge piers and slit structures has been examined experimentally as well as numerically (1) and (2). Recently, the interactions among driftwoods have been taken into account in the numerical models, since their interactions are closely related to the entrapment and accumulation around hydraulic structures.

In terms of the local phenomena, the relationships between driftwoods and hydraulic structures can be interpreted as the mechanical interactions between the floating objects in free-surface flows and the fixed objects. While some flexible branches and grass may be related to the entrapment of the driftwoods in the actual problems, the flexibility is neglected in the present study and our focus is placed on the mechanical relationships of rigid bodies. Thus, the driftwoods are modeled as the rigid bodies. In particular, the advanced rigid models will be developed and the interactions with free-surface flows will be investigated in the present study.

In the usual computational models, driftwoods are sometimes represented by the group of the spheres used in DEM (3) in order to deal with their collisions easily. This type of models is called "sphere-connection-model"

in this paper. One of the problems of the sphere-connection-model is the inaccuracy in the representation of the geometries of driftwoods. In our previous study (4), it was shown that the volume, mass and inertia tensors are not accurately represented with the sphere-connection-model.

To solve such problems involved in the sphere-connection-models, the T-type solid model was proposed by Ushijima et al. (5). In the T-type model, an object is represented with multiple tetrahedron elements. Although, in the sphere-connection-model, the clearances and penetrations arise among sphere elements, the tetrahedron elements enable us to represent the target object more accurately and to obtain for the volume, mass and inertia tensors more exactly as shown by Ushijima et al. (6). In addition, since the T-type solid model uses "contact-spheres", which are placed inside of the object surfaces to detect collisions and to evaluate the contact forces, the numerical procedures for the collision-detection are easy compared with those of the polygon models such as a GJK model (7).

The T-type solid model is introduced into the computational method for multiphase fields, MICS (8). As a result, the interactions between the objects and free-surface flows, such as fluid forces and torques acting on the objects, can be treated adequately through the tetrahedron sub-cell method. This computational method was applied to the transportation and entrapment of driftwoods. The predicted movements of the driftwoods were compared with the experimental results and the applicability of the prediction method was discussed.

NUMERICAL PROCEDURES

It is necessary to employ the numerical methods that enable us to deal with the interactions between floating objects and free-surface flows in order to predict the transportation of driftwoods. In the computational method for multiphase fields, MICS, it has been demonstrated that the natural frequencies and stabilities of floating objects can be evaluated accurately (9). On the basis of MICS, a computational method is developed to predict the transportation of driftwoods in the present study.

Computational method for free-surface flows

The governing equations in MICS, which were proposed by Ushijima et al. (8), are shown as follows:

$$\frac{\partial \rho}{\partial t} + \frac{\partial}{\partial x_j}(\rho u_j) = 0 \tag{1}$$

$$\frac{\partial u_j}{\partial x_j} = 0 \tag{2}$$

$$\frac{\partial u_i}{\partial t} + \frac{\partial}{\partial x_j}(u_i u_j) = f_i - \frac{1}{\rho}\frac{\partial p}{\partial x_i} + \frac{1}{\rho}\frac{\partial}{\partial x_j}\left[\frac{\partial}{\partial x_j}(\mu u_i) + \frac{\partial}{\partial x_i}(\mu u_j)\right] \tag{3}$$

where t and x_i are time and a coordinate in three-dimensional orthogonal coordinates ($i = 1, 2, 3$). Eq.1 is the mass conservation equation in Eulerian description, Eq.2 is the incompressible condition and Eq.3 is the momentum equation in the preservation form. The volume-averaged density, the viscous coefficient and pressure are denoted by ρ, μ and p, respectively, while u_i is the mass-averaged velocity component and f_i is the acceleration component of the external force. The surface tensions between the different phases are assumed to be negligible in this paper.

The numerical procedures to obtain approximate solutions for the governing equations are similar to those for the incompressible fluids based on a MAC method. Firstly, the volume fraction of the object included in a fluid-cell is evaluated through the tetrahedron sub-cell method (10) and the volume-averaged variables are determined.

Then, on the basis of the numerical algorithms for incompressible fluids with the collocated grid system, after the tentative velocity components are calculated in the cell-center points from convection and diffusion terms (prediction stage), the tentative values are spatially interpolated on the cell-boundaries to solve pressure-Poisson equations with C-HSMAC method (11) (pressure-computation stage). The implicit computational method, C-ISMAC method (12), is utilized in the prediction stage to improve the computational efficiency. The free-surface profiles are calculated by solving Eq.1 with the fifth-order TVD scheme (13) and a numerical filter to prevent the numerical diffusion.

T-type solid model representing drift wood

After the pressure and velocity fields are obtained, the fluid forces acting on the objects are calculated to evaluate the motions of the objects. The driftwoods are assumed to be rigid bodies and they are treated with the T-type solid model (5). Since in the T-type rigid model, the object is represented by multiple tetrahedron elements, the inertia tensors and fluid forces are evaluated more accurately than the usual sphere-connection-model. In addition, since the shape of the object is created with a CAD software and then the element division is performed with a mesh-generating software, the T-type solid model enables us to treat the complicated-shape driftwoods with the accurate shapes. In the present investigation, however, the driftwoods have the simple cylindrical shapes to compare the predicted results with the experimental values.

Fig.1 illustrates the tetrahedron elements of the T-type solid model representing the cylindrical driftwood used in the experiments, which is 20 mm in diameter and 100 mm in length. The number of the tetrahedron elements in Fig.1 is 682.

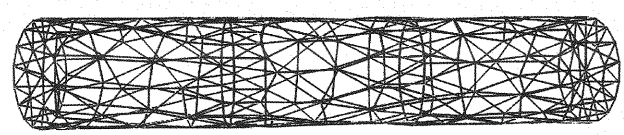

Fig. 1 T-type solid model for driftwood used in experiments

The inertia tensors are evaluated with the following procedures: Firstly, the inertia tensor $\boldsymbol{I}_n$ is calculated with respect to one vertex C_n of the tetrahedron element n, whose mass is M_n. Then, the derived value is transformed to the inertia tensor $\boldsymbol{I}_{tn}$ on the basis of the center of the element as shown by Ushijima et al. (6).

$$\boldsymbol{I}_{tn} = \boldsymbol{I}_n - M_n \boldsymbol{F}(\boldsymbol{r}_c) \tag{4}$$

where $\boldsymbol{F}(\boldsymbol{r})$ is given by

$$\boldsymbol{F}(\boldsymbol{r}) = \begin{bmatrix} r_2^2 + r_3^2 & -r_1 r_2 & -r_1 r_3 \\ -r_2 r_1 & r_1^2 + r_3^2 & -r_2 r_3 \\ -r_3 r_1 & -r_3 r_2 & r_1^2 + r_2^2 \end{bmatrix} \tag{5}$$

and $\boldsymbol{r}_c$ in Eq.4 is the vector directing from the vertex C_n to the center of the element. Secondly, $\boldsymbol{I}_{tn}$ is transformed to the inertia tensor $\boldsymbol{I}_{0n}$ based on the center of the object with the following equation:

$$\boldsymbol{I}_{0n} = \boldsymbol{I}_{tn} + M_n \boldsymbol{F}(\boldsymbol{r}_c + \boldsymbol{r}_n) \tag{6}$$

where $\boldsymbol{r}_n$ denotes the vector from the center of the object to the vertex C_n of the tetrahedron element. The inertia tensor of the object $\boldsymbol{I}$ is obtained by taking the summation of $\boldsymbol{I}_{0n}$ over all elements consisting of the

object. On the other hand, the mass of the T-type solid model is easily evaluated as the summation of those of the tetrahedron elements. When the approximation for the geometry is sufficiently accurate, the above physical properties can be evaluated adequately.

Movements of T-type solid model

Since the driftwoods are assumed to be rigid bodies in the present study, the movements can be divided into the rotational and translational motions. Thus, as shown in Fig.2, the initial attitude of the object is defined as the "basic-attitude" and the position and attitude at a specific time are determined with the rotation of the basic-attitude and the translational motion of the rotated object.

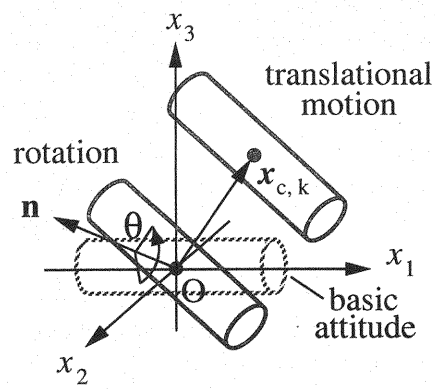

Fig. 2 Schematic view of rigid body motion

The basic equation for the translational motion is given by

$$M\dot{\boldsymbol{v}} = \boldsymbol{F} \tag{7}$$

where M is the mass of the object, $\boldsymbol{v}$ is the velocity vector of the object center point and the dot represents the time differentiation. The external force $\boldsymbol{F}$ is determined by the fluid forces and the contact forces due to collisions with boundaries and other objects.

On the other hand, the rotating motion of the object follows the Euler's equation of momentum:

$$\dot{\boldsymbol{L}} = \boldsymbol{N} \tag{8}$$

where $\boldsymbol{N}$ is the torque acting on the rigid body and $\boldsymbol{L}$ is the angular momentum vector. The angular momentum vector $\boldsymbol{L}$ can be expressed as follows:

$$\boldsymbol{L} = R\boldsymbol{I}\boldsymbol{\omega} \tag{9}$$

where $\boldsymbol{I}$ denotes the inertia tensor of the object in the basic-attitude, $\boldsymbol{\omega}$ is the angular velocity vectors for basic-attitude and R is the rotation matrix which transforms the object in the basic-attitude to the present attitude. By differentiating Eq.9 with respect to time, the following equation is derived:

$$\dot{\boldsymbol{L}} = \dot{R}\boldsymbol{I}\boldsymbol{\omega} + R\boldsymbol{I}\dot{\boldsymbol{\omega}} \tag{10}$$

where $\dot{R}$ is given as follows:

$$\dot{R} = RQ(\boldsymbol{\omega}) \tag{11}$$

with

$$Q(\boldsymbol{\omega}) = \begin{bmatrix} 0 & -\omega_3 & \omega_2 \\ \omega_3 & 0 & -\omega_1 \\ -\omega_2 & \omega_1 & 0 \end{bmatrix} \tag{12}$$

where ω_i is the i component of the angular velocity vector $\boldsymbol{\omega}$. With the $Q(\boldsymbol{\omega})$ and the relationship $Q(\boldsymbol{\omega})\boldsymbol{I\omega} = \boldsymbol{\omega} \times \boldsymbol{I\omega}$, Eq.8 is rewritten as

$$R(\boldsymbol{\omega} \times \boldsymbol{I\omega} + \boldsymbol{I\dot{\omega}}) = \boldsymbol{N} \tag{13}$$

From Eq.13, the angular acceleration vector $\dot{\boldsymbol{\omega}}$ is given by

$$\dot{\boldsymbol{\omega}} = \boldsymbol{I}^{-1}\left[R^{-1}\boldsymbol{N} - \boldsymbol{\omega} \times \boldsymbol{I\omega}\right] \tag{14}$$

In the actual computation, quaternions are utilized to evaluate $R^{-1}\boldsymbol{N}$ instead of the rotation matrix R as proposed by Ushijima et al. (6). After determining the right hand side of Eq.14 in this way, $\boldsymbol{\omega}$ is obtained by the numerical time integration. Since the derived $\boldsymbol{\omega}$ is the angular velocity vector for the basic-attitude, it is transformed to $\boldsymbol{\omega}_n$ for the present attitude with the quaternions. After completing the above procedures, the present attitude is determined using the quaternions in the same direction as the rotation axis $\boldsymbol{\omega}_n$ and the angle of the rotation $|\boldsymbol{\omega}_n|\Delta t_b$, where Δt_b is the time increment in the computation of the object motions.

Fluid forces and Contact forces acting on T-type solid model

The fluid forces acting on the T-type solid model are evaluated from the pressure and viscous terms in Eq.3. The volume fraction of the object k included in a fluid-cell C, which is defined as α_{Ck}, is used in this procedure. Fig.3 shows the relationship between the fluid-cell and tetrahedron elements of the driftwood model. In Fig.3, the portion of the tetrahedron element included in the fluid-cell is depicted by a colored area. In order to evaluate the volume of this area, the tetrahedron sub-cell method (10) is utilized.

The fluid force $\boldsymbol{F}_{Ck}$ acting on the colored area shown in Fig.3 is determined with the terms in Eq.3, α_{Ck}, the volume of a fluid-cell and the density of the object. The fluid force acting on the center of the object is obtained from the summation of $\boldsymbol{F}_{Ck}$. In addition, the torque acting on the colored area due to the fluid force is determined as the exterior product of the vector $\boldsymbol{r}_{GC}$, directing from the center of the object $\boldsymbol{x}_G$ to the center of the fluid-cell $\boldsymbol{x}_C$, and $\boldsymbol{F}_{Ck}$. The torque against the object is defined as the summation of $\boldsymbol{r}_{GC} \times \boldsymbol{F}_{Ck}$.

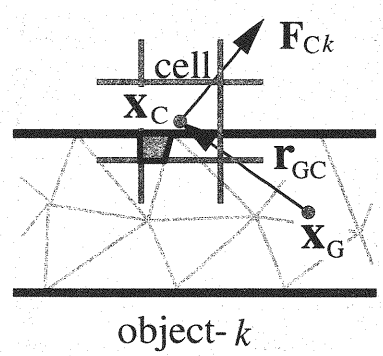

Fig. 3 Fluid force and torque acting on T-type solid model

On the other hand, the contact forces due to collisions with the boundaries and the other objects are evaluated with the contact-spheres in the T-type solid model. Fig.4 shows the distribution of the contact-spheres for the driftwood model. The distributions and sizes of the contact-spheres can be determined arbitrarily, since they are not used to evaluate the physical properties such as mass, inertia tensors and fluid forces. In the present study, the center points of the contact-spheres are placed at the center of the tetrahedron elements, which are faced with the object surfaces as done in our previous study (5). The diameter of each contact-sphere is determined so that its volume is equivalent to that of the corresponding element.

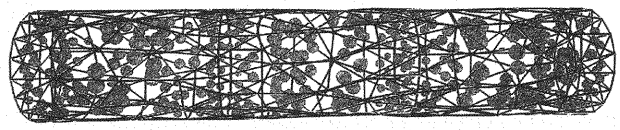

Fig. 4 Distribution of contact-spheres in T-type solid model

APPLICABILITY OF THE PREDICTION METHOD

The transportation of the driftwood models and their entrapment around piers were experimentally investigated with the water tank shown in Fig.5. The length L and width B in Fig.5 are 400 mm and 190 mm respectively and the water depth is 150 mm. The inlet and outlet are equipped on the left and right sides respectively on the bottom surface of the tank and the circulating flows were generated by the pump. The flow rate was set at 220 cm^3/s in all experiments. Near the free surface, the flows in the direction from left to right sides were created and five driftwood models, whose diameter and length are 20 mm and 100 mm respectively, were transported by the flows.

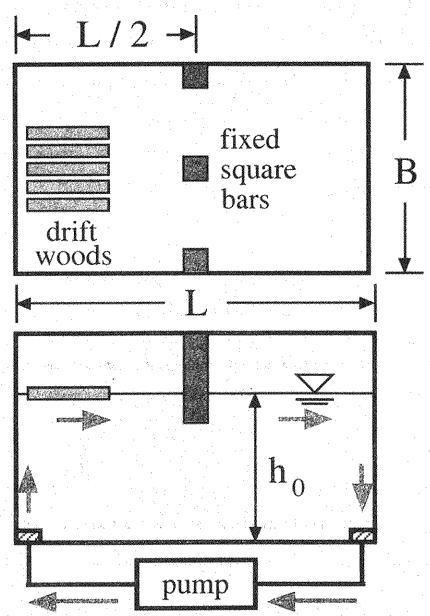

Fig. 5 Experimental tank (plane and side views)

The multiple piers are fixed in the middle of the tank as shown in Fig.5. The tops of the piers are fixed and their bottom is located at 20 mm below the free surface. The cross section of each pier is a square of 20 × 20 mm. Some of the released driftwood models were trapped in front of the piers and others were transported through the clearances between piers. In these experiments, the behaviors of the driftwood models were observed by changing the number of piers from three to five.

Fig.6 and Fig.7 show the behaviors of the driftwood models in the experiments. In the case where the number of the piers was five, most of the driftwood models were trapped in front of the piers due to the narrower clearances, while a few of them passed through the piers in cases where the pier number was four.

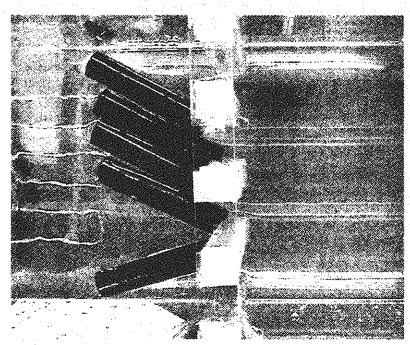

Fig. 6 Experimental results (five piers)

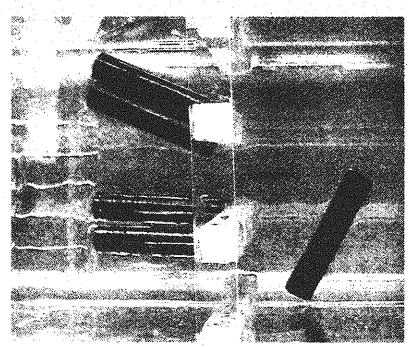

Fig. 7 Experimental results (four piers)

Fig.8 and Fig.9 show the predicted results with five and four piers respectively. The number of the fluid-cells is 40 × 19 × 20 in call calculations. The unsteady computations were performed for 10 seconds and the final distributions of the driftwoods were obtained. The computational time in each case was about 85 minutes (Pentium4, 2.66GHz). As shown in Fig.8, all driftwoods are trapped by the piers with five piers, while one driftwood passes through them in cases where there are four piers.

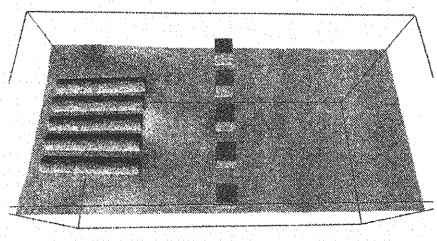

$t = 1.0$ (s)

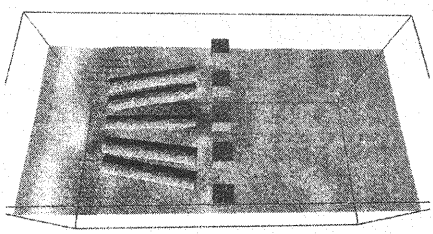

$t = 2.0$ (s)

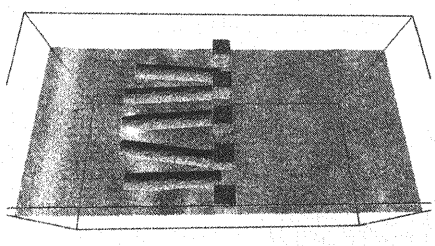

$t = 3.0$ (s)

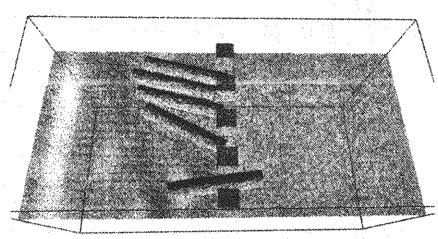

$t = 10.0$ (s)

Fig. 8 Predicted behaviors of driftwoods (five piers)

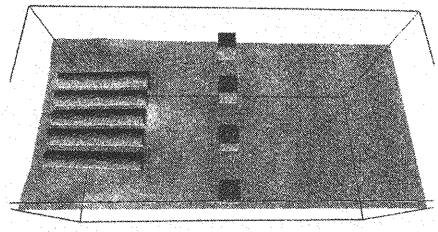

$t = 1.0$ (s)

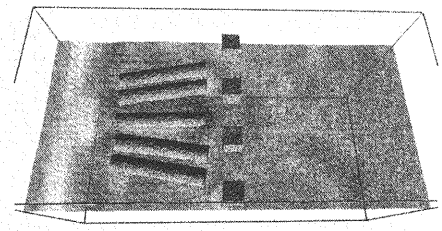

$t = 2.0$ (s)

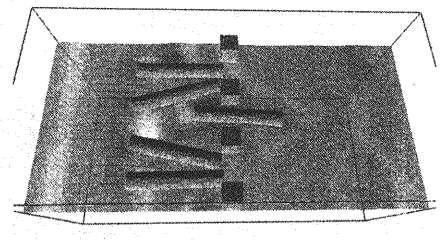

$t = 3.0$ (s)

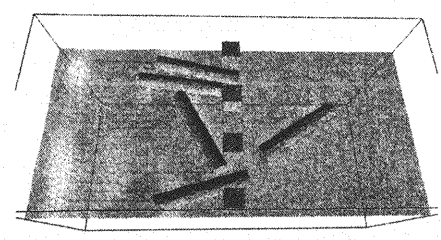

$t = 10.0$ (s)

Fig. 9 Predicted behaviors of driftwoods (four piers)

Fig.10 and Fig.11 show the experimental and predicted results respectively with three piers. As shown in these figures, a greater number of driftwoods are transported through the piers when the clearances increase.

The number of the driftwoods that pass through the piers are summarized in Tab.1. The experimental results in Tab.1 are obtained as the averaged values from more than 10 times observations. While the predicted number of the passing driftwoods is greater than that of the experiments in three piers, the predicted results are in good agreement with the experimental values in the other cases.

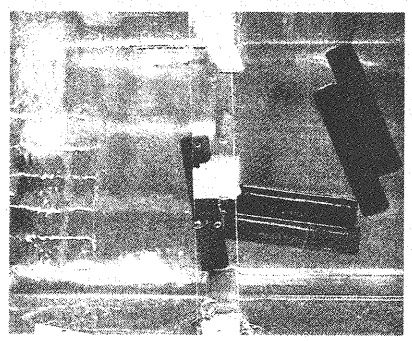

Fig. 10 Experimental results (three piers)

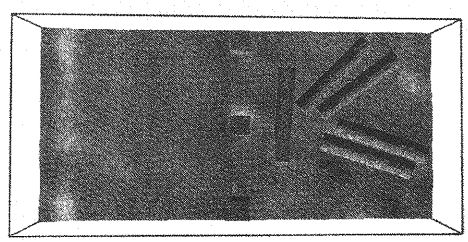

Fig. 11 Predicted results (three piers)

Table 1 Number of passing driftwoods

number of piers	3	4	5
clearance (mm)	65.0	27.5	22.5
experiments	2.8	0.87	0.10
computations	5	1	0

In the experiments, driftwood models stick slightly to the piers and other models probably due to the effects of the surface tension. This tendency causes the difference between predictions and experiments in case that the number of the piers is three in Tab.1. It is, however, thought that the effects of the surface tension become less in the actual phenomena which have larger scales than experiments.

CONCLUSIONS

The computational method was developed to predict the transportation and entrapment of driftwoods around piers. The prediction method is based on the MICS, which enables us to deal with multiphase fields accurately, such as the free-surface flows including the floating objects. The driftwoods are treated as rigid bodies with the T-type solid model, in which an object is represented with multiple tetrahedron elements and contact-spheres are used in the collision detections. The prediction method was applied to the experimental results and the behaviors of the driftwoods were compared. As a result, while slight differences were found between them in case that the surface tensions were not negligible, it was found that the numbers of the driftwoods that pass through the piers can be generally predicted adequately with the present method.

REFERENCES

1. Ikari, H., Gotoh, H. and Sumi, T.: Computational mechanics of a blocking of gateless bottom outlet by drift woods, *Annu. J. Hydraulic Eng., JSCE*, Vol. 50, pp. 793–798, 2006.
2. Shimizu, Y., Osada, K. and Takanashi, T.: Numerical simulation of the driftwoods behavior by using a DEM-flow coupling model, *Annu. J. Hydraulic Eng., JSCE*, Vol. 50, pp. 787–792, 2006.
3. Cundall, P. A. and Strack, O. D. L.: A discrete numerical model for granular assemblies, *Geotechnique*, Vol. 29, No. 1, pp. 47–65, 1979.
4. Fujioka, S. and Ushijima, S.: Numerical prediction of fluid fields with arbitrary-shaped solid bodies with MICS, *Annu. J. Hydraulic Eng., JSCE*, Vol. 50, pp. 751–756, 2006.
5. Ushijima, S., Fukutani, A., Makino, O. and Nezu, I.: Computational method for arbitrarily-shaped solid models moving in 3D flows with collisions and deformations, *J. Applied Mech., JSCE*, Vol. 10, pp. 139–146, 2007.
6. Ushijima, S., Fukutani, A., Fujioka, S. and Nezu, I.: Numerical prediction method for arbitrarily-shaped bodies moving in three-dimensional fluids, *Annu. J. Hydraulic Eng., JSCE*, Vol. 51, pp. 847–852, 2007.
7. Glbert, E. G., Johnson, D. W. and Keerthi, S. S.: A fast procedure for computing the distance between complex objects in three-dimensional space, *IEEE Journal of Robotics and Automation*, Vol. 4, No. 2, pp. 193–564, 1988.
8. Ushijima, S., Yamada, S., Fujioka, S. and Nezu, I.: Prediction method (3D MICS) for transportation of solid bodies in 3D free-surface flows, *JSCE Journal*, Vol. 810/II-74, pp. 79–89, 2006.
9. Fukutani, A., Ushijima, S., Makino, O. and Nezu, I.: Applicability of multiphase-flow solver (3D MICS) to movements of floating objects, *J. Applied Mech., JSCE*, Vol. 10, pp. 705–712, 2007.
10. Ushijima, S., Makino, O. and Nezu, I.: 3D numerical prediction for flood flows into residential area with tetrahedron sub-cell method, *Annu. J. Hydraulic Eng., JSCE*, Vol. 51, pp. 787–792, 2007.
11. Ushijima, S., Okuyama, Y., Takemura, M. and Nezu, I.: Parallel computational method for pressure field in incompressible flows on 3D curvilinear coordinates, *Annual Journal of Hydraulic Engineering, JSCE*, Vol. 47, pp. 385–390, 2003.
12. Ushijima, S. and Nezu, I.: Higher-order implicit (C-ISMAC) method for incompressible flows with collocated grid system, *JSCE Journal*, No. 719/II-61, pp. 21–30, 2002.
13. Yamamoto, S. and Daiguji, H.: Higher-order-accurate upwind schemes for solving the compressible Euler and Navier-Stokes equations, *Computers Fluids*, Vol. 22, No. 2/3, pp. 259–270, 1993.

APPENDIX-NOTATION

The following symbols are used in this paper:

C = fluid-cell;
C_n = vertex of tetrahedron element;
$\boldsymbol{F}$ = external force vector;
$\boldsymbol{F}(\boldsymbol{r})$ = tensor given by Eq.5;
$\boldsymbol{F}_{Ck}$ = fluid force vector acting on the colored area in Fig.3;
f_i = acceleration of external force in x_i direction;
$\boldsymbol{I}$ = inertia tensor of object;
$\boldsymbol{I}_{0n}$ = inertia tensor of element based on center of object;
$\boldsymbol{I}_n$ = inertia tensor of element based on its vertex;
$\boldsymbol{I}_{tn}$ = inertia tensor of element based on its center;
$\boldsymbol{L}$ = angular momentum vector;
$\dot{\boldsymbol{L}}$ = time-differentiation of angular momentum vector;
M = mass of object;
M_n = mass of tetrahedron element;
$\boldsymbol{N}$ = torque acting on object;
p = volume-averaged pressure;
$Q(\boldsymbol{\omega})$ = matrix given by Eq.12;
R = rotation metrix;
$\dot{R}$ = time-differentiation of R;
$\boldsymbol{r}$ = position vector;
r_i = i component of $\boldsymbol{r}$;
$\boldsymbol{r}_{GC}$ = vector from $\boldsymbol{x}_G$ to $\boldsymbol{x}_C$;
$\boldsymbol{r}_c$ = vector from C_n to $\boldsymbol{x}_C$;
$\boldsymbol{r}_n$ = vector from $\boldsymbol{x}_G$ to C_n;
t = time;
u_i = mass-averaged velocity component in x_i direction;
$\boldsymbol{x}_C$ = center of tetrahedron element;
$\boldsymbol{v}$ = velocity vector of object;
$\dot{\boldsymbol{v}}$ = time-differentiation of $\boldsymbol{v}$;
$\boldsymbol{x}_G$ = center of object;
x_i = orthogonal coordinates;
α_{Ck} = volume fraction of tetrahedron elements in fluid-cell;
Δt = time increment;
μ = volume-averaged coefficient of viscosity;
ρ = volume-averaged fluid density;
$\boldsymbol{\omega}$ = angular velocity vector; and
ω_i = i component of $\boldsymbol{\omega}$.

(Received Jul 14, 2008 ; revised Jan 06, 2009)